Electronic Supplementary Information

for the manuscript
"Controlled Nitrene Transfer from a Tyrosinase-Like Arylnitroso-Copper Complex"

by
Mohammad S. Askari, Maylis Orio and Xavier Ottenwaelder*
* dr.x@concordia.ca

Experimental Procedures

Chemicals were obtained from Sigma-Aldrich and Alfa Aesar, except acetanilide-^{15}N from Cambridge Isotope Laboratories. Air-sensitive compounds were handled under inert atmosphere (N_2) in a dry nitrogen glove-box (O_2 < 0.1 ppm, H_2O < 0.1 ppm) or using standard Schlenk techniques. Solvents were dried by standard procedures, degassed, and stored over 4 Å molecular sieves in the glove-box. *N,N,N',N'*-tetramethyl-1,3-propanediamine (TMPD) was distilled over CaH_2 under nitrogen, and stored in the glove-box. The copper salt [$(MeCN)_4Cu$](TfO) was prepared by adapting the Kubas procedure using TfOH.[1] 4-nitrosonitrobenzene was prepared via a literature procedure.[2] Sodium 2,4-di-*tert*-butylphenolate was prepared in the glove-box by treating recrystallized 2,4-di-*tert*-butylphenol with NaH in THF followed by filtering off the solids and precipitating with diethyl ether. NMR spectra were recorded on Varian Innova-500 MHz instrument. IR spectra were recorded on a Nicolet iS5 (Thermo Scientific) ATR. UV-vis spectra were recorded on Agilent 8453 spectrophotometer.

Preparation of *p*-NO_2-$C_6H_4{}^{15}NO$:

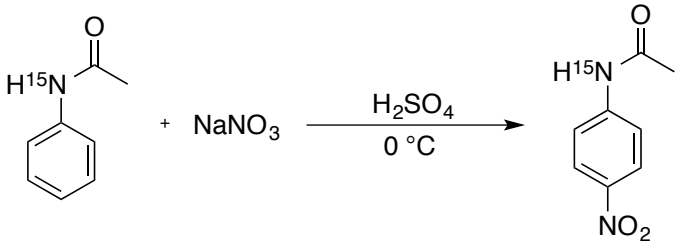

(a) *p*-nitroacetanilide-^{15}N. Acetanilide-^{15}N was nitrated by adapting a literature procedure.[3] To a solution of acetanilide-^{15}N (500 mg, 3.7 mmol) in 6 mL of concentrated H_2SO_4 at 0 °C, a solution of $NaNO_3$ (313 mg, 3.7 mmol, 1 equiv.) in 4 mL concentrated H_2SO_4 was added dropwise over 20 minutes. The mixture was left stirring for 5 hours at 0 °C and then poured onto ice-water mixture. The yellow precipitated solid was filtered off and washed with water and used for next step without further purification. Yield: 563 mg, 85%. ^{1}H-NMR (acetone-d_6): δ (ppm) 9.80-9.62 (d, 1H, -C^{15}N*H*-, $^1J_{H\text{-}^{15}N}$ = 90 Hz), 8.22-8.21 (d, 2H, Ar-*H*), 7.91-7.89 (d, 2H, Ar-*H*), 2.17 (s, 3H, -C(O)C*H*$_3$).

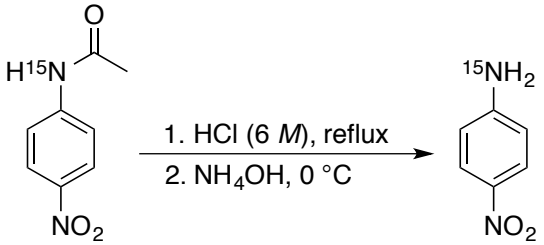

(b) *p*-nitroaniline-^{15}N. *p*-nitroacetanilide-^{15}N (563 mg, 3.1 mmol) was dissolved in 20 mL of 6 M HCl and the solution refluxed for 24 hours. The solution was then cooled to 0 °C and basified by adding NH_4OH upon which yellow crystals formed which were filtered off and washed with cold water. Yield: 416 mg, 96%. ^{1}H-NMR ($CDCl_3$): δ (ppm) 8.08-8.06 (m, 2H, Ar-*H*), 6.63-6.62 (m, 2H, Ar-*H*), 4.39 (d, 2H, $^{15}NH_2$, $^1J_{H\text{-}^{15}N}$ = 86Hz).

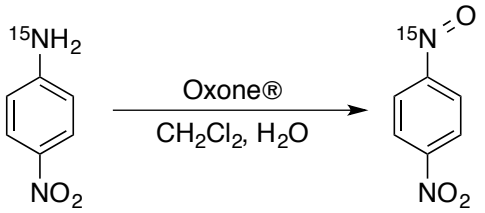

(c) *p*-(^{15}N-nitroso)nitrobenzene. Oxidation of *p*-nitroaniline-^{15}N was carried out following a literature procedure.[2] To a solution of *p*-nitroaniline-^{15}N (400 mg, 2.9 mmol) in 20 mL of CH_2Cl_2 at 25 °C a solution of Oxone® ($2KHSO_5 \bullet KHSO_4 \bullet K_2SO_4$, 3.9g, 6.3 mmol, 2.2 equiv.) in 10 mL of water was added and the mixture stirred vigorously. The progress of the reaction was monitored by TLC until all the starting material was consumed. The organic phase was separated and the aqueous layer was extracted twice with CH_2Cl_2. The combined organic layer was washed once with 1 M aqueous HCl, dried over Na_2SO_4, filtered, and solvent removed under reduced pressure to give brown solid. The crude product was purified by sublimation under vacuum to afford green crystals of the nitrosoarene that dimerized at 25 °C over few hours. Yield: 220 mg, 50%. ^{1}H-NMR ($CDCl_3$): δ (ppm) 8.52-8.51 (m, 2H, Ar-*H*), 8.06-8.04 (m, 2H, Ar-*H*). ^{13}C{^{1}H}-NMR (125 MHz, $CDCl_3$): 162.43 (d, $^1J^{13}_{C\text{-}}{}^{15}_{N}$ = 13.3Hz), 125.5, 124.9, 121.3 (d, $^2J^{13}_{C\text{-}}{}^{15}_{N}$ = 4.3Hz). ^{15}N{^{1}H}-NMR (50 MHz, $CDCl_3$): 913.8

Preparation of {[(TMPD)Cu]$_2$(TfO)(μ-η^2:η^2-*p*-NO$_2$-C$_6$H$_4$NO)}(TfO), 1: to a stirring solution of TMPD (40 mg, 0.31 mmol, 1.2 equiv.) and 4-nitrosonitrobenzene (46 mg , 0.30 mmol, 0.7 equiv.) in 5 mL THF, a solution of [(MeCN)$_4$Cu](TfO) (100 mg, 0.26 mmol, 1 equiv.) in 2 mL THF was added dropwise at 25 °C. The color changed immediately to deep green. The solution was stirred for 15 minutes and then cooled down to –30 °C. Dropwise addition of the solution to 15 mL of swirling pentane previously cooled to –30 °C resulted in the precipitation of a green solid. The solid was isolated and washed with Et_2O, pentane and dried in vacuo. Yield: 80%. ^{1}H-NMR (acetone-d_6): δ (ppm) 8.26-8.17 (m, 4H, aromatic), 2.82 (bs, 4H, N–CH_2), 2.72 (bs, 24H, N(CH_3)$_2$), 1.93 (bs, 4H, CH_2–CH_2–CH_2). UV-Vis λ_{max} / nm (ε / $M^{-1}cm^{-1}$): 346 (19 400), 445 (4 400, shoulder), 643 (1 500). Elemental analysis: calculated for $C_{22}H_{40}N_6O_9F_6S_2Cu_2$, C 31.54, H 4.81, N 10.03, S 7.65; found C 31.60, H 2.03*, N 9.81, S 7.81. * The presence of fluorine in the sample interfered with the normal integration peak for hydrogen. The value for H is not trustworthy.
Crystals suitable for X-ray structure determination were grown through slow layered diffusion of pentane into a concentrated solution of the complex in THF at –30 °C.

Preparation of complex 2 (reaction of 1 with phenolate): To a solution of **1** (86.7 mg, 0.1 mmol, 1 equiv.) in 10 mL CH_2Cl_2, solid sodium 2,4-di-*tert*-butylphenolate (25.6 mg, 0.1 mmol, 1 equiv.) was added at 25 °C. Within a few minutes the color of the solution changed from green to deep blue. After stirring for 1 h, the solution was filtered through a 0.45 μM PTFE syringe filter. Fast precipitation through dropwise addition of the solution into stirring pentane precooled to –30 °C gave blue microcrystalline solid of **2**, which was collected and dried under vacuum. Yield: 76%. ^{1}H-NMR ($CDCl_3$): δ 8.47 (d, 2H), 7.67 (s, 1H), 7.64 (d, 2H), 6.40 (s, 1H), 3.09 (t, 4H), 2.59 (bs, 12H), 1.87 (bs, 2H), 1.51 (s, 9H), 1.13 (s, 9H). UV-Vis λ_{max} / nm (ε / $M^{-1}cm^{-1}$): 328 (8 100), 556 (2 800, shoulder), 713 (7 500). Elemental analysis: calculated for $C_{28}H_{42}N_4O_6F_3SCu \cdot 0.2CH_2Cl_2$,* C 48.37, H 6.10, N 8.00, S 4.58; found C 48.03, H 6.33, N 8.14, S 5.08. * 80% of the crystallization solvent evaporated when drying the sample.
X-ray quality crystals were grown by layered diffusion of pentane into a concentrated solution of the complex in CH_2Cl_2 at –30 °C.

***N*-(2-hydroxyphenyl)-4-nitroaniline, 3:** To a solution of **1** (86.7 mg, 0.1 mmol, 1 equiv.) in 10 mL CH_2Cl_2, solid sodium 2,4-di-*tert*-butylphenolate (25.6 mg, 0.1 mmol, 1 equiv.) was added at 25 °C. Within a few minutes the colour of the solution changed from green to deep blue. To this solution a saturated solution of $Na_2S_2O_4$ was added under Ar upon which the color changed to light yellow, at which stage the solutions were handled in the air. The aqueous phase was then extracted twice more with CH_2Cl_2, organics combined, dried over Na_2SO_4, filtered, and solvent removed under reduced pressure to give a yellow oil. Purification by silica gel column (hexanes/ethyl acetate) provided the pure title compound as pale yellow solid. Yield: 80%. ^{1}H-NMR (CDCl3): δ (ppm) 8.10-8.08 (d, 2H), 7.30 (s, 1H), 7.03 (s, 1H), 6.68-6.66 (d, 2H), 5.86 (bs, 1H), 5.74 (bs, 1H), 1.44 (s, 9H), 1.28 (s, 9H). ^{13}C{^{1}H}-NMR (125 MHz, $CDCl_3$): δ (ppm) 152.5, 148.8, 143.0, 140.2, 136.4, 126.2, 125.3, 123.3, 121.6, 113.7, 35.1, 34.4, 31.5, 29.5. IR (ATR, cm^{-1}): 3466, 3327, 2954, 1589, 1481, 1420, 1362, 1297, 1216, 1181, 1110, 974, 839, 751, 697, 652. HRMS: m/z calculated for $[M+H]^+$, 343.20217; found, 343.20135.

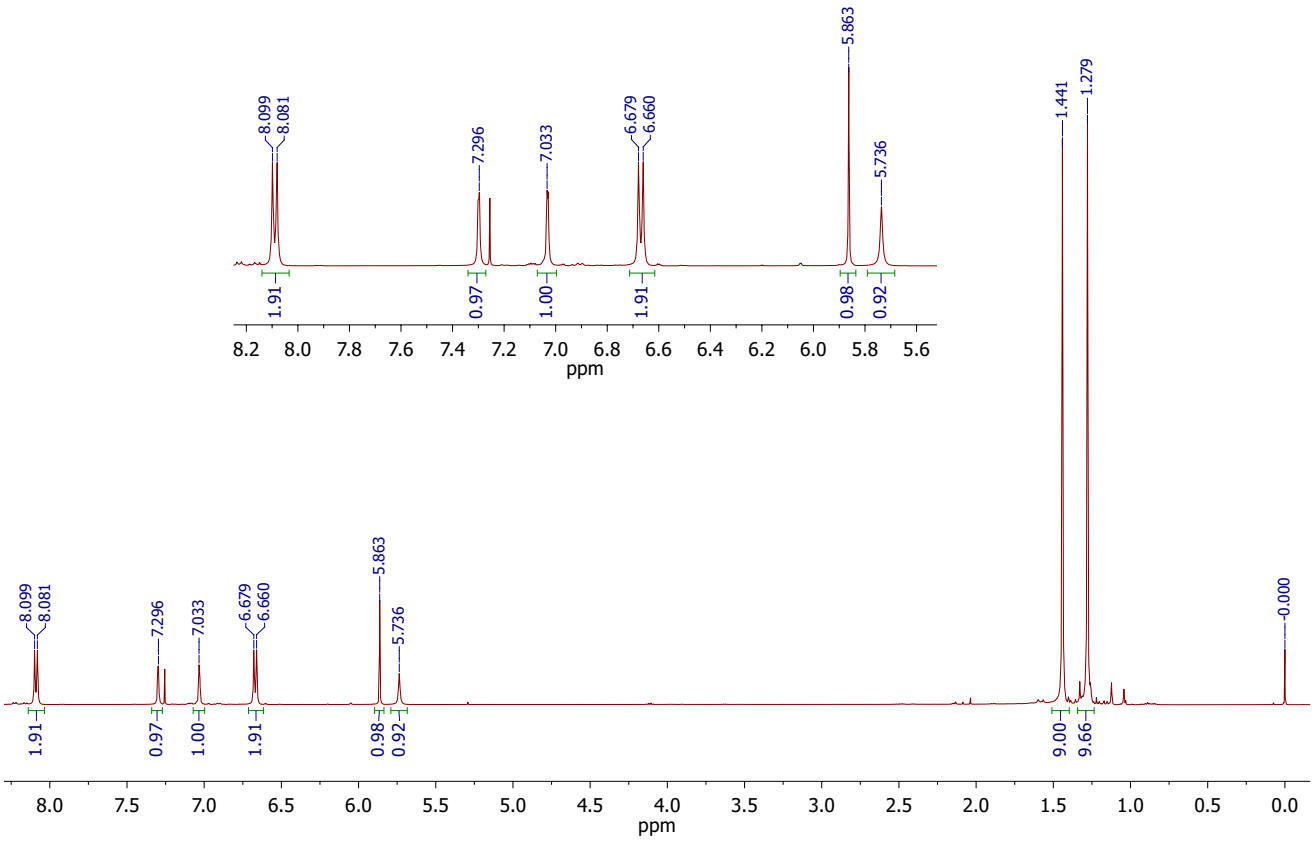

Figure S1. ^{1}H NMR spectrum of **3** ($CDCl_3$, 25 °C).

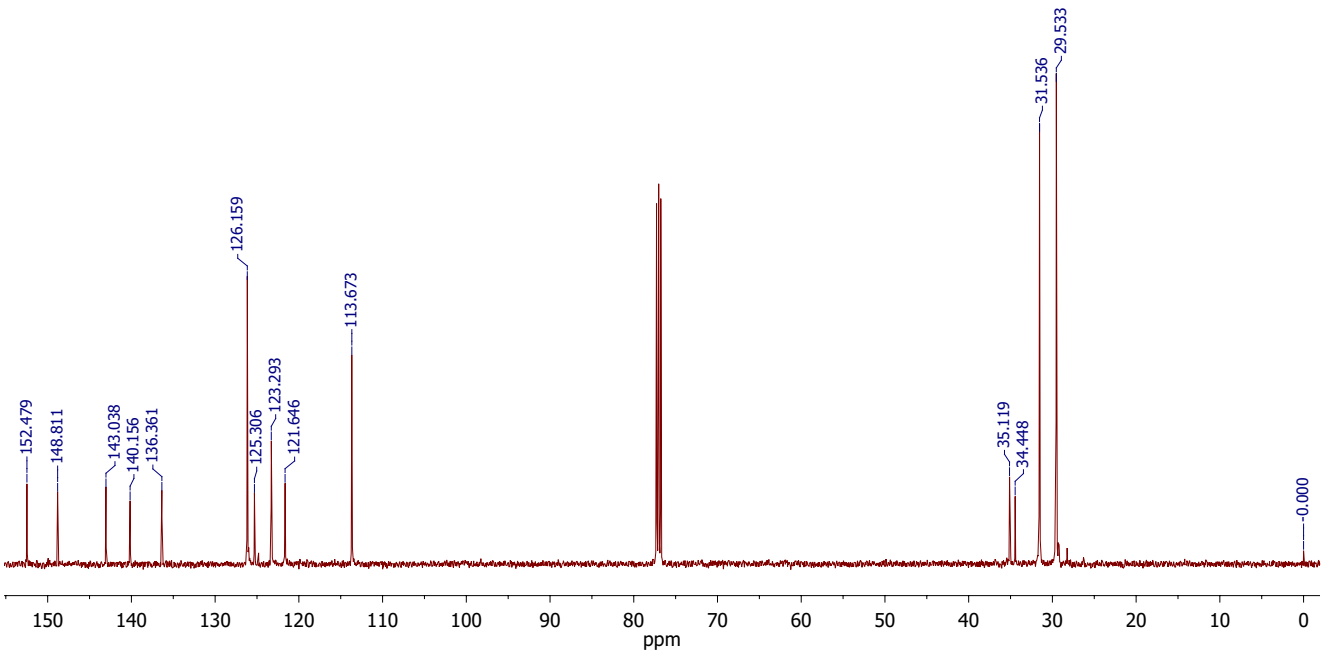

Figure S2. $^{13}C\{^{1}H\}$ NMR spectrum of **3** ($CDCl_3$, 25 °C).

X-ray Crystallography

X-ray diffraction data were collected on a Bruker APEX DUO used micro-focused copper source. The frames were integrated with the Bruker SAINT software package using a narrow-frame algorithm. The Data were corrected for absorption effects using the multi-scan method (SADABS). The structure was solved and refined using the Bruker SHELXTL Software Package. The final anisotropic full-matrix least-squares refinement is on F^2.

Table S1. Crystallographic data for [**1**](TfO) and [**2**](TfO)·CH_2Cl_2.

	[**1**](TfO)	[**2**](TfO)·CH_2Cl_2.
CCDC deposition number	1029423	1029424
Empirical formula	$C_{22}H_{40}Cu_2F_6N_6O_9S_2$	$C_{29}H_{44}Cl_2CuF_3N_4O_6S$
Formula weight	837.80	768.18
T (K)	110(2)	113(2)
Wavelength (Å)	1.54178	1.54178
Crystal system	orthorhombic	orthorhombic
Space group	$P2_12_12_1$	Pbcn
Unit cell dimensions		
a (Å)	12.6647(4)	34.9331(5)
b (Å)	15.6022(7)	10.1199(2)
c (Å)	17.2534(8)	20.5135(3)
α (°)	90.00	90.00
β (°)	90.00	90.00
γ (°)	90.00	90.00
V (Å^3)	3409.2(2)	7251.9(2)
Z	4	8
D_{calc}	1.632	1.407
Absorption coefficient	3.478	3.262
F(000)	1720	3200
Crystal size (mm)	0.073 x 0.107 x 0.124	0.07 x 0.30 x 0.38
θ (°)	3.820 – 62.746	2.53 – 68.16
Index ranges	h = -14 – 14	h = -41 – 41
	k = -17 – 17	k = -12 – 12
	l = -19 – 19	l = -24 – 23
Reflections collected	45388	99756
Independent reflections	5454	6605
Completeness (θ)	99.4%	99.6%
Data/restraints/parameters	5454/0/433	6605/19/453
Goodness of fit (GOF) on F^2	1.021	1.049
Final R indices [$I > 2\sigma(I)$] (%)	R_1 = 5.02, wR_2 = 10.43	R_1 = 5.27, wR_2 = 14.23
R indices (all data) (%)	R_1 = 8.67, wR_2 = 12.04	R_1 = 7.21, wR_2 = 15.61
Largest difference in peak and hole (e Å^{-3})	0.552 and -0.493	1.214 and -1.148

UV-Vis Spectra

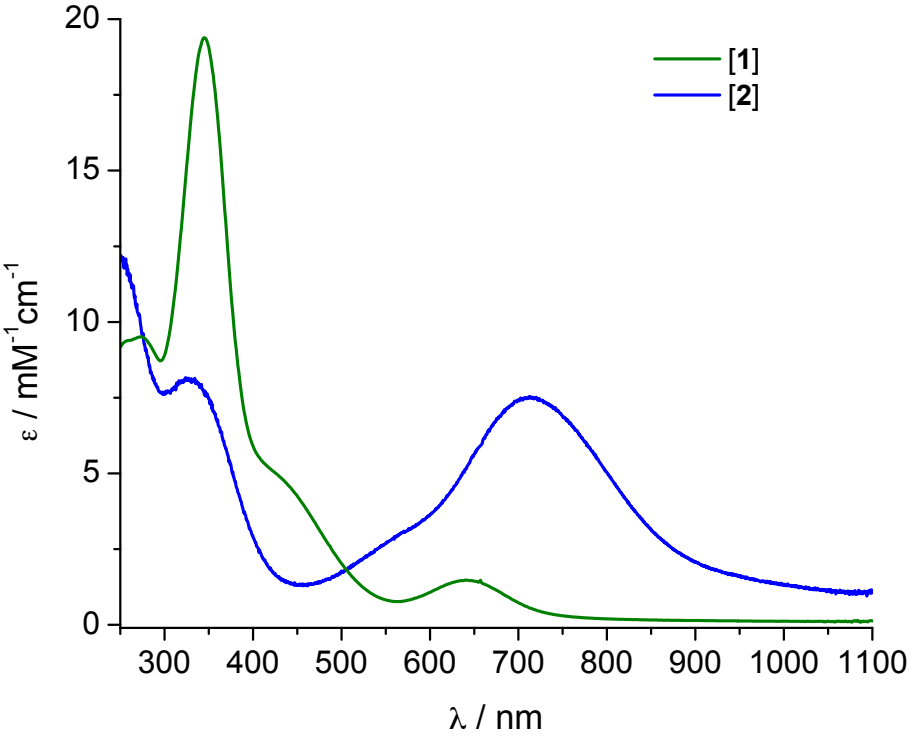

Figure S3. UV-Vis spectra of **1** and **2** in CH_2Cl_2 at 25 °C.

IR Spectra and Vibrational Analysis

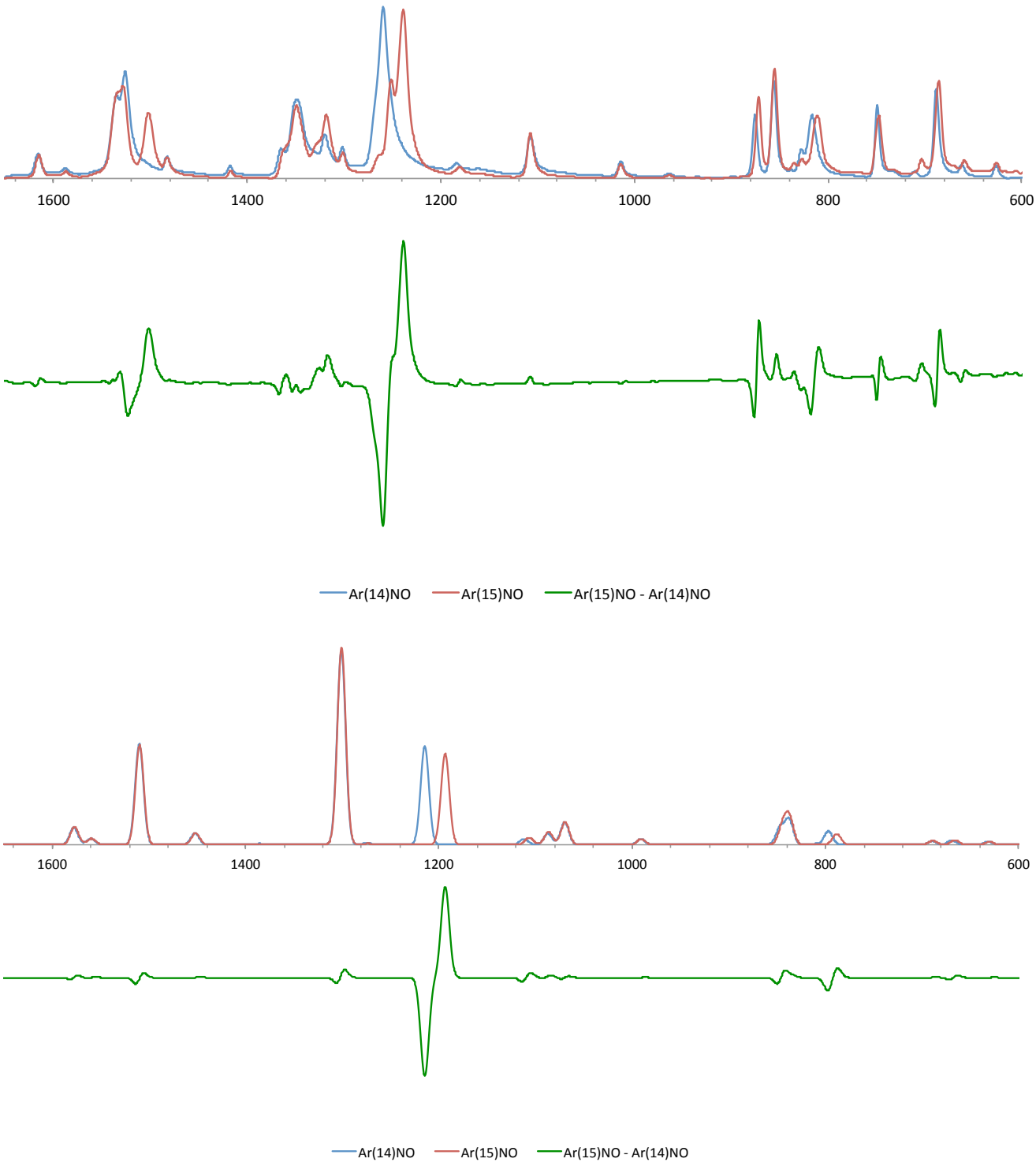

Figure S4. Experimental (top) and computational (bottom, see below for details) IR spectra for solid *p*-(^{14}N-nitroso)nitrobenzene (blue), *p*-(^{15}N-nitroso)nitrobenzene (red), and difference spectra (green).

Table S2. Selected calculated IR parameters for $Ar^{14/15}NO$ (dimer form).

$Ar^{14}NO$		**$Ar^{15}NO$**		Assignment
Freq. (cm^{-1})	Intensity (a.u.)	Freq. (cm^{-1})	Intensity (a.u.)	
796.9	62.6	788.2	49.1	δ_r NN + δ_r CH_{Ar}
1214.5	443.9	1193.4	409.7	ν_s NO + ν_s CH_{Ar}

Computational details below. ν_s: streching, δ_b: bending, δ_r: rocking, δ_w: wagging, δ_t: twisting

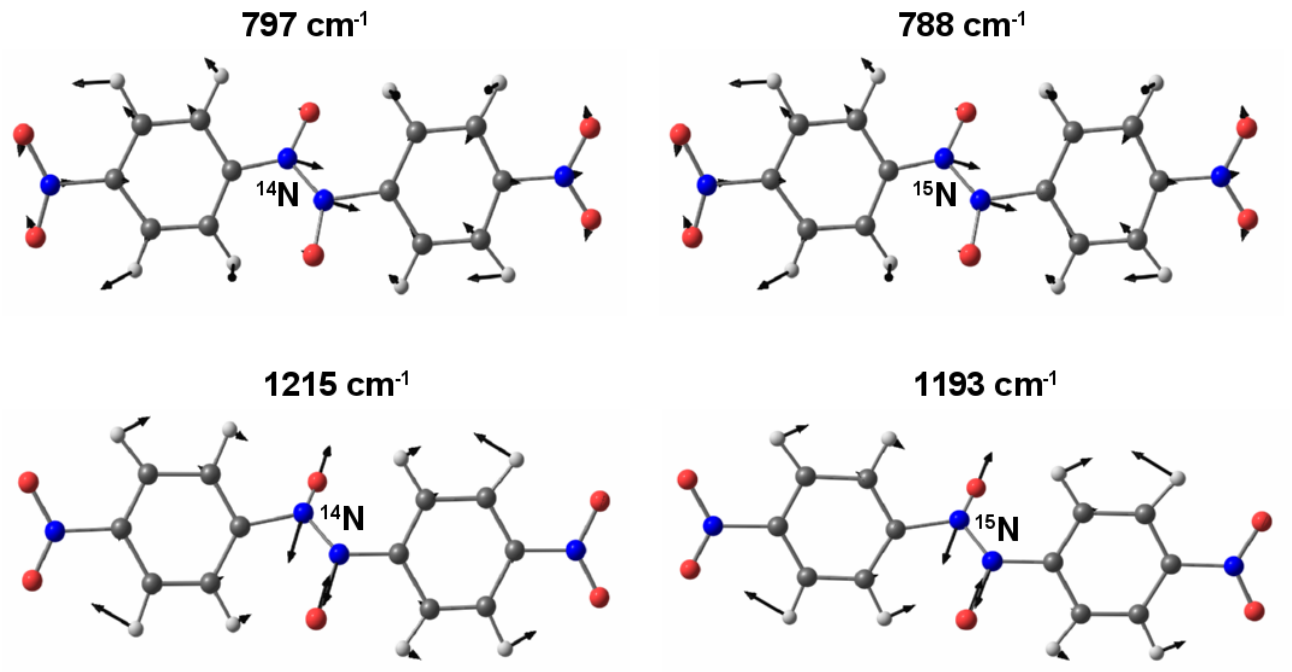

Figure S5. Relevant vibrational normal modes of $Ar^{14/15}NO$, a dimer in the solid-state structure.

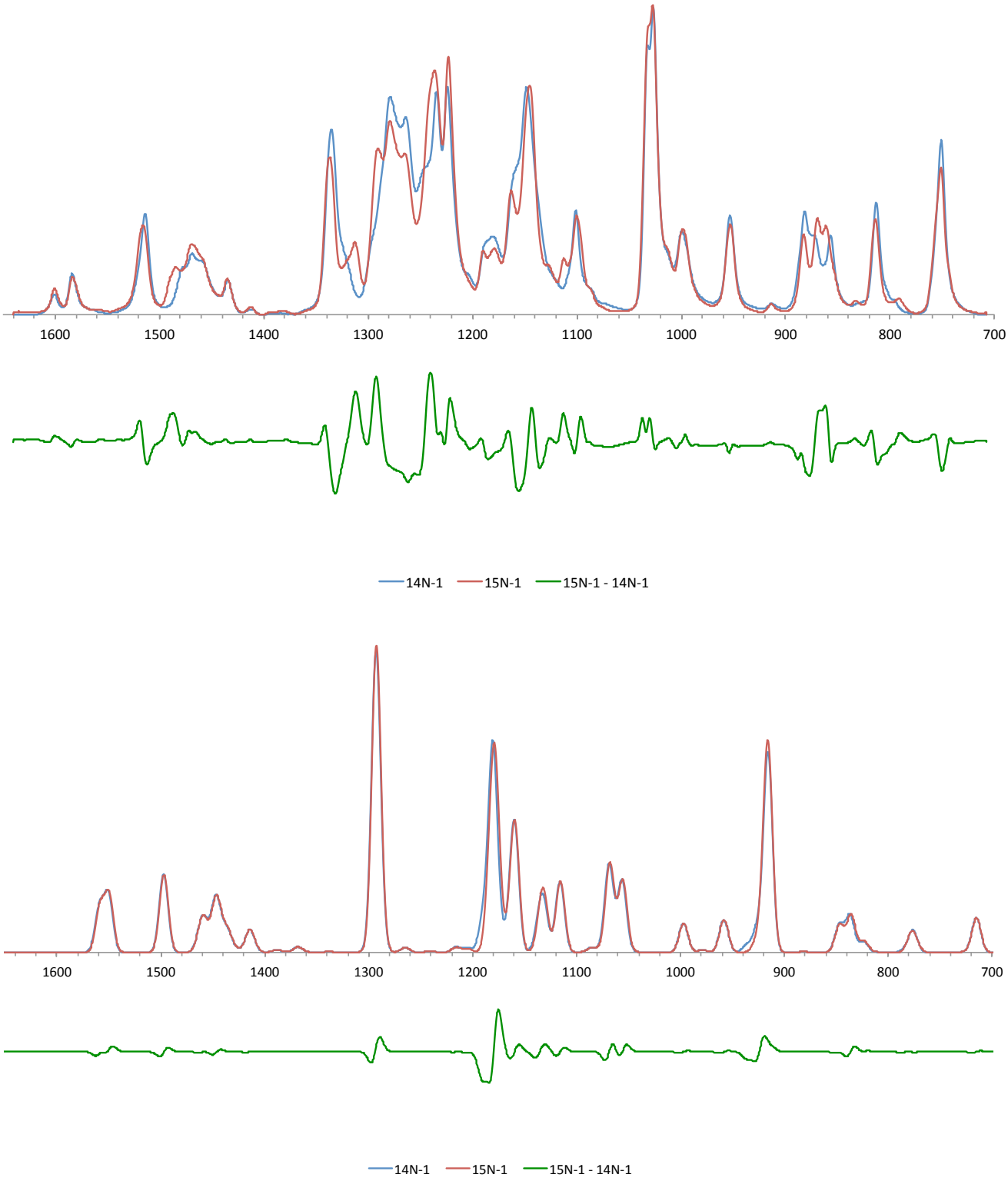

Figure S6. Experimental (top) and computational (bottom, see below for details) IR spectra for **1**-^{14}N (blue), **1**-^{15}N (red), and difference spectra (green).

Table S3. Selected calculated IR parameters for **1**.

^{14}N-1		^{15}N-1		Assignment
Freq. (cm^{-1})	Intensity (a.u.)	Freq. (cm^{-1})	Intensity (a.u.)	
935.9	60.3	918.8	87.8	ν_s NO
1189.7	71.1	1183.7	109.0	ν_s N_{NO}-C_{Ar} + ν_s CH_{Ar}

Computational details below. ν_s: streching, δ_b: bending, δ_r: rocking, δ_w: wagging, δ_t: twisting

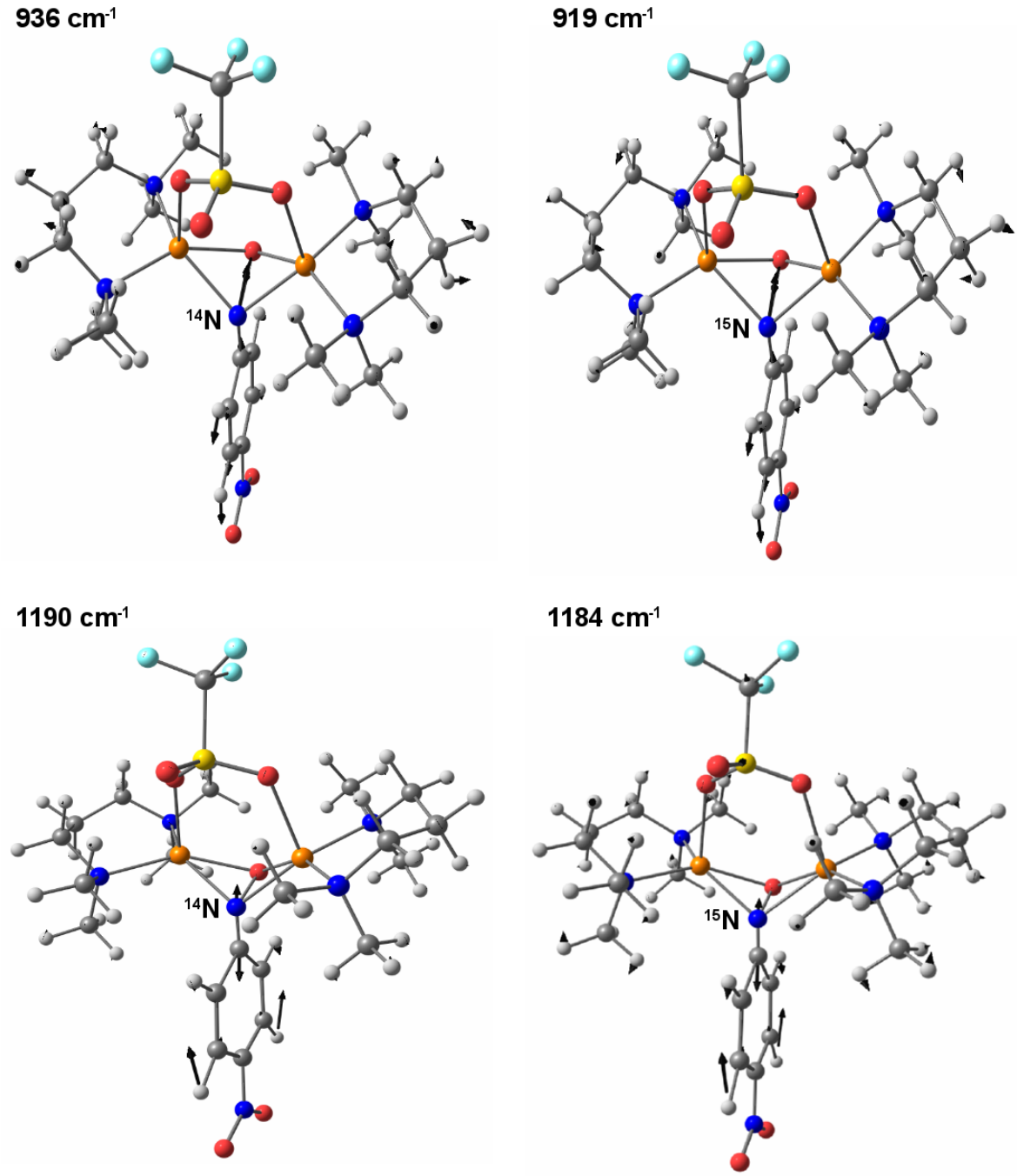

Figure S7. Relevant vibrational normal modes of ^{14}N- and ^{15}N-labeled **1**.

DFT calculations

All theoretical calculations were performed with the ORCA program package.[4] Full geometry optimizations were carried out for all complexes using the GGA functional BP86[5-7] in combination with the TZV/P[8] basis set for all atoms and by taking advantage of the resolution of the identity (RI) approximation in the Split-RI-J variant[9] with the appropriate Coulomb fitting sets.[10] Increased integration grids (Grid4 in ORCA convention) and tight SCF convergence criteria were used. Solvent effects were accounted for according to the experimental conditions. For that purpose, we used the CH_2Cl_2 (ε = 9.08) solvent within the framework of the conductor like screening (COSMO) dielectric continuum approach.[11] The relative energies were obtained from single-point calculations using the B3LYP[12,13] functional together with the TZV/P basis set. They were computed from the gas-phase optimized structures as a sum of electronic energy, thermal corrections to free energy, and free energy of solvation. The Heisenberg isotropic exchange coupling constants *J* were evaluated from single point calculations based on the Broken Symmetry (BS) approach[14-16] using the B3LYP functional and the TZV/P basis set. The Yamaguchi formula [17,18] was used to estimate the exchange coupling constants *J* based on the Heisenberg–Dirac–van Vleck Hamiltonian[19-22] Optical properties were predicted from additional single-point calculations using the same functional/basis set as employed before. Electronic transition energies and dipole moments for all models were calculated using time-dependent DFT (TD-DFT)[23-25] within the Tamm-Dancoff approximation.[26,27] To increase computational efficiency, the RI approximation[28] was used in calculating the Coulomb term. At least 40 excited states were calculated in each case and difference transition density plots were generated for each transition. IR spectra were obtained from numerical frequency calculations performed on optimized structures using the B3LYP functional together with the TZV/P basis set. Isotope shift effects ($^{14}N/^{15}N$) were taken into account using the orca_vib utility program. Vibrational normal modes were visualized with Chemcraft[29] software and differential spectra were plotted using the orca_maspc utility program.

Complex 1

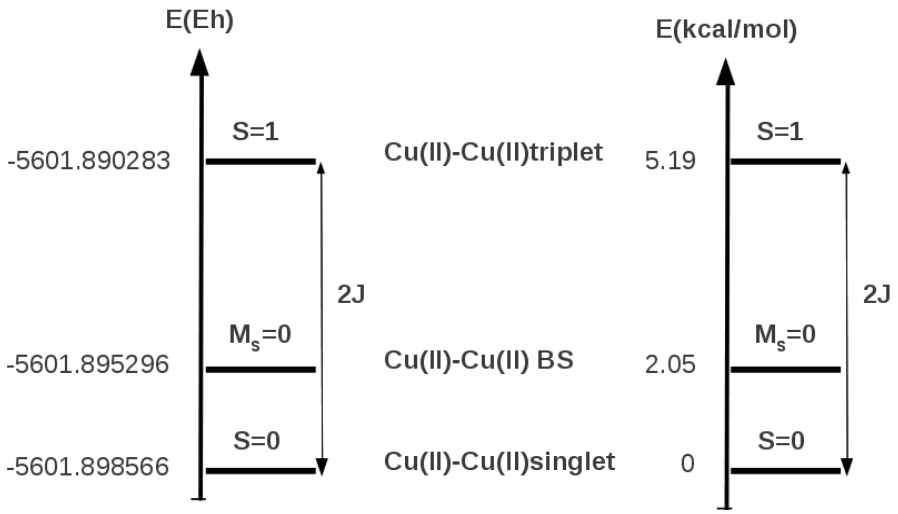

Figure S8. Energetic analysis of the DFT calculations for **1**.

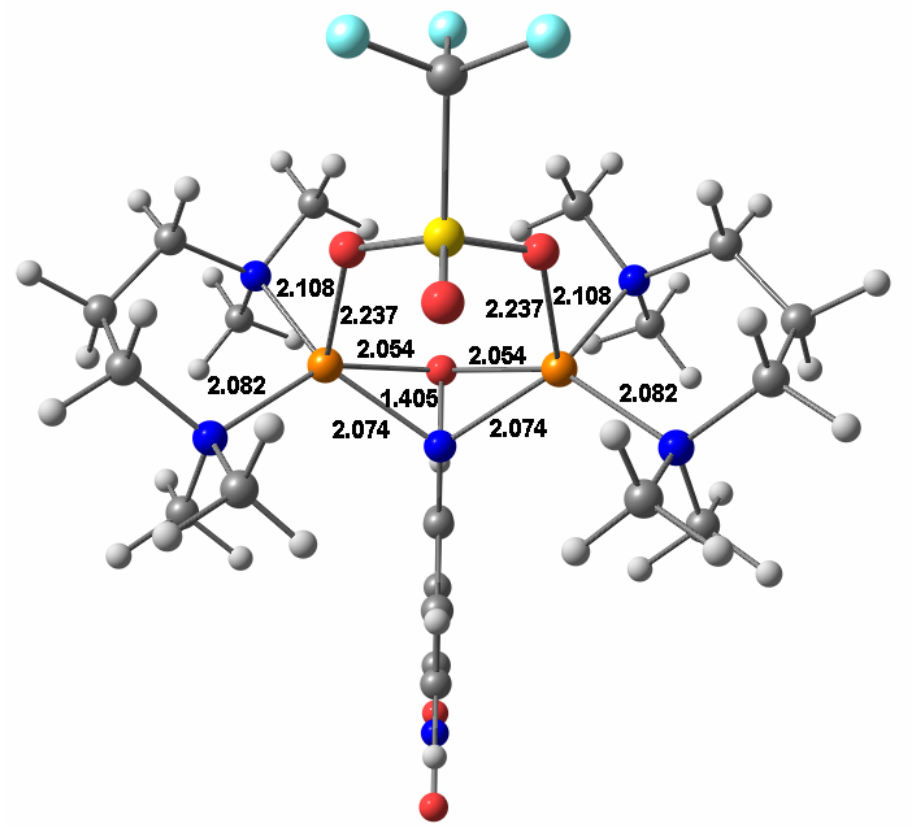

Figure S9. Optimized structure of cation **1** together with interatomic distances.

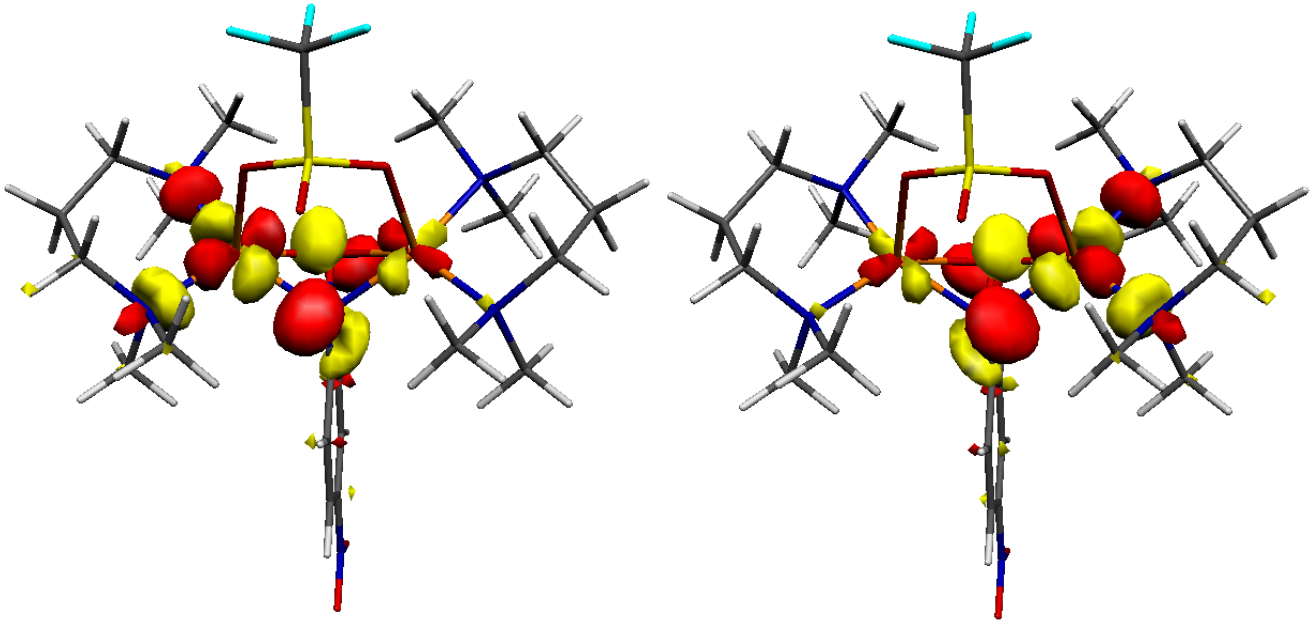

Figure S10. Unrestricted corresponding orbitals of **1**.

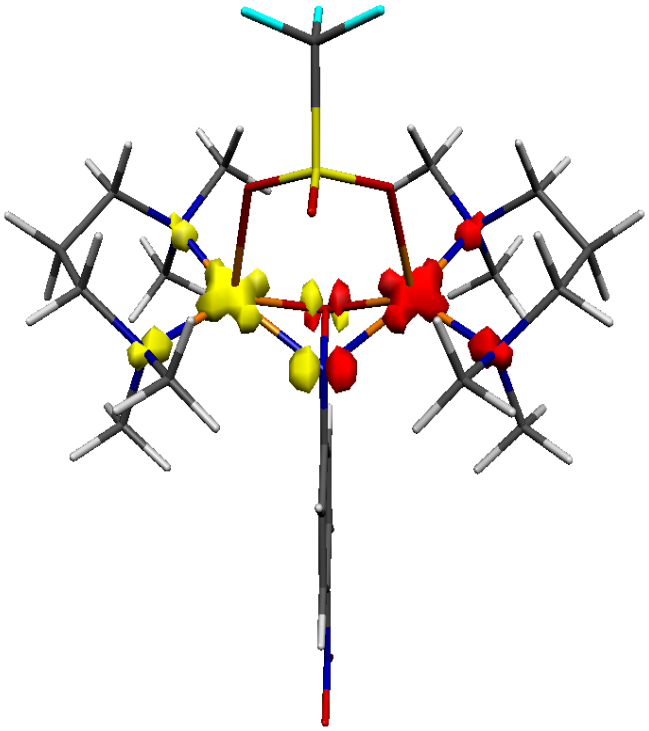

Figure S11. Spin population distribution in **1**.

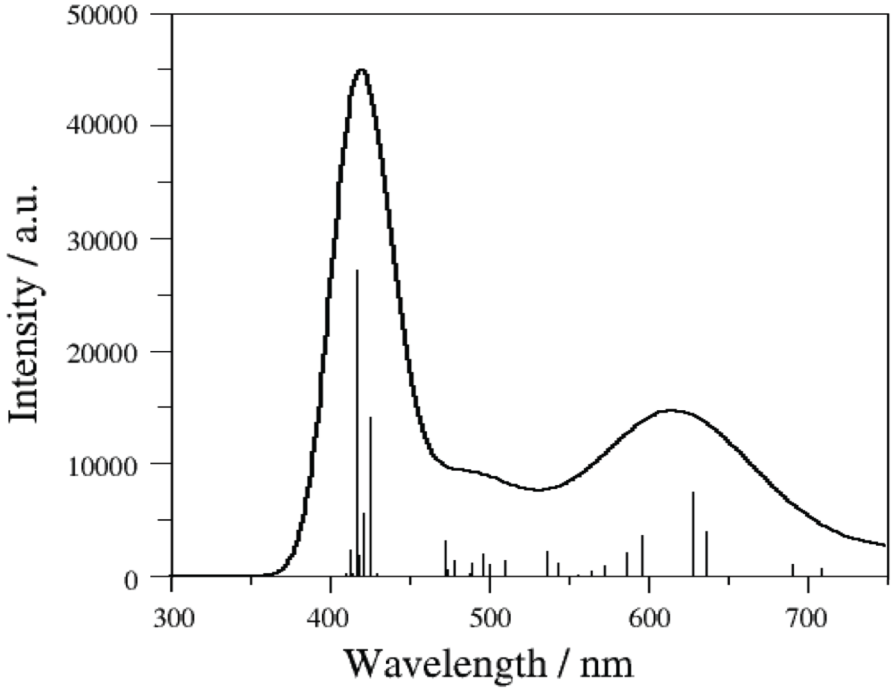

Figure S12. Theoretical fit of the UV-vis spectrum of **1**.

Table S4. Calculated electronic transitions of **1**.

Transition	λ^{calc} (nm)	f^{calc}	Assignment	λ^{expt} (nm)	ε (M^{-1} cm^{-1})
1	664	0.126	MLCT	643	1500
2	454	0.095	LLCT	445	4400
3	418	0.272	MLCT	346	19400

Transition 1

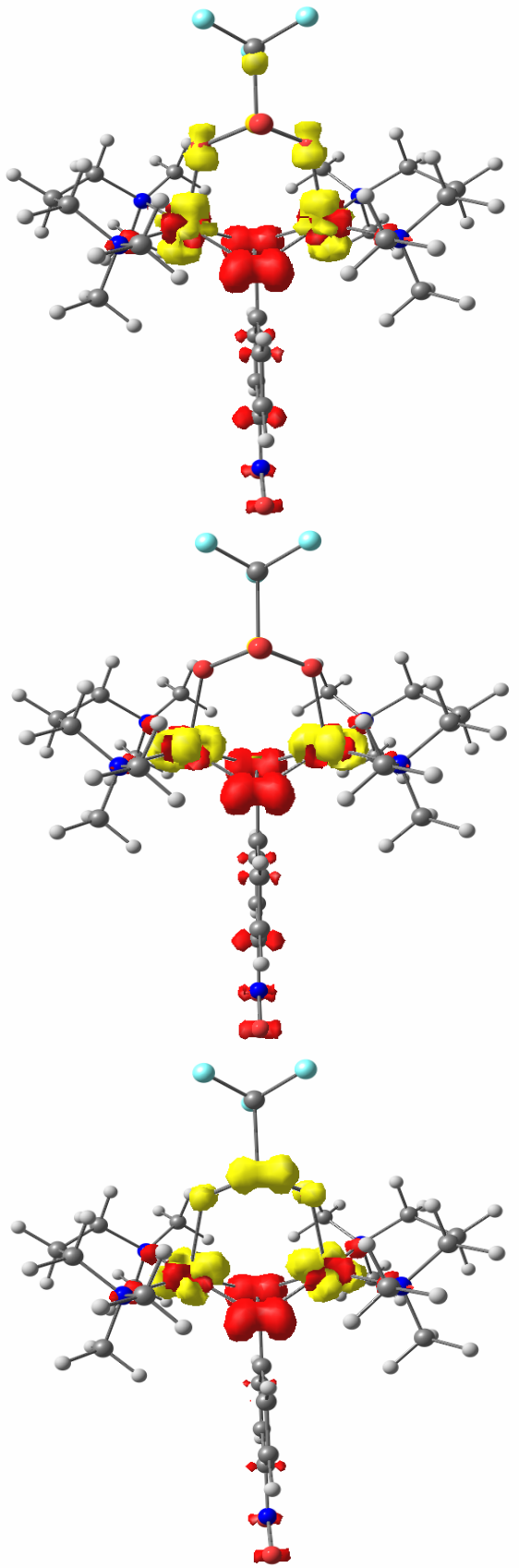

Transition 2

Transition 3

Figure S13. Difference electron densities sketch of transitions 1-3 for **1** (yellow = negative, red = positive).

Peroxo analogue of 1

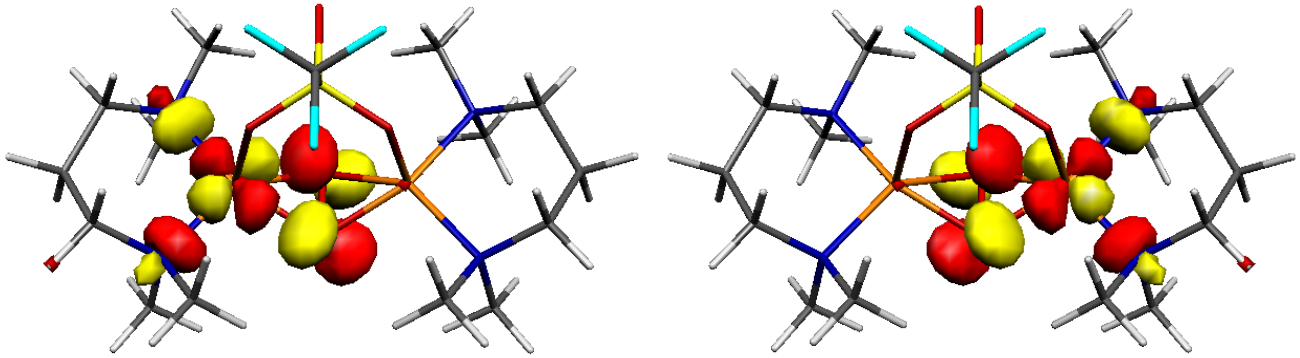

Figure S14. Unrestricted corresponding orbitals for peroxo analogue of **1**.

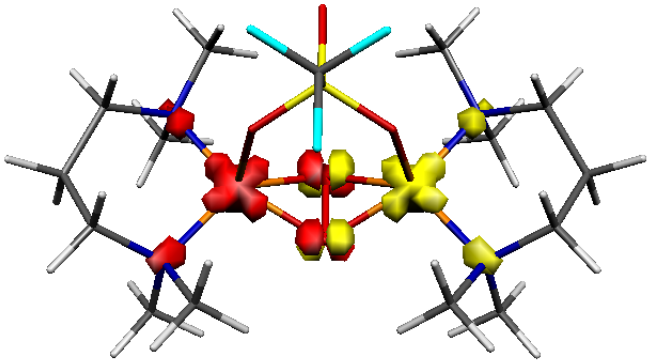

Figure S15. Spin population distribution for peroxo analogue of **1**.

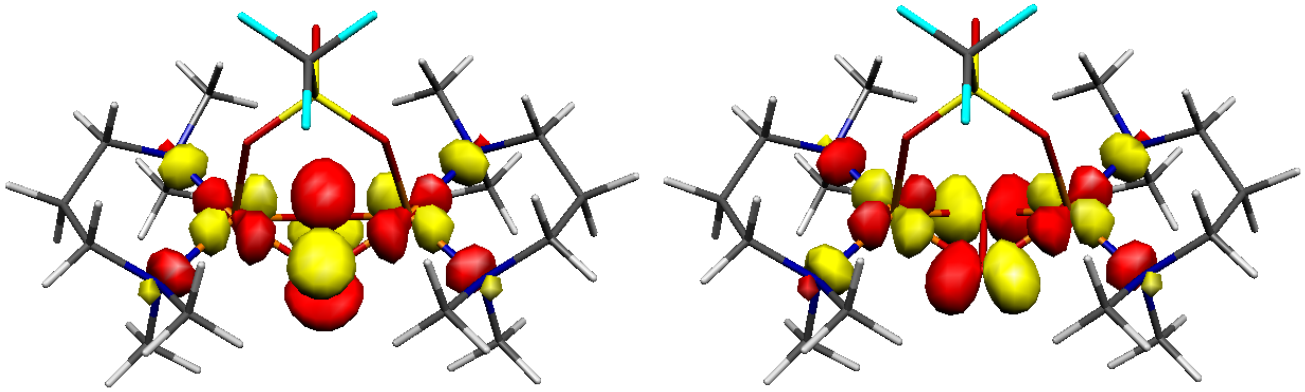

Figure S16. HOMO (left) and LUMO (right) for peroxo analogue of **1**.

Complex 2

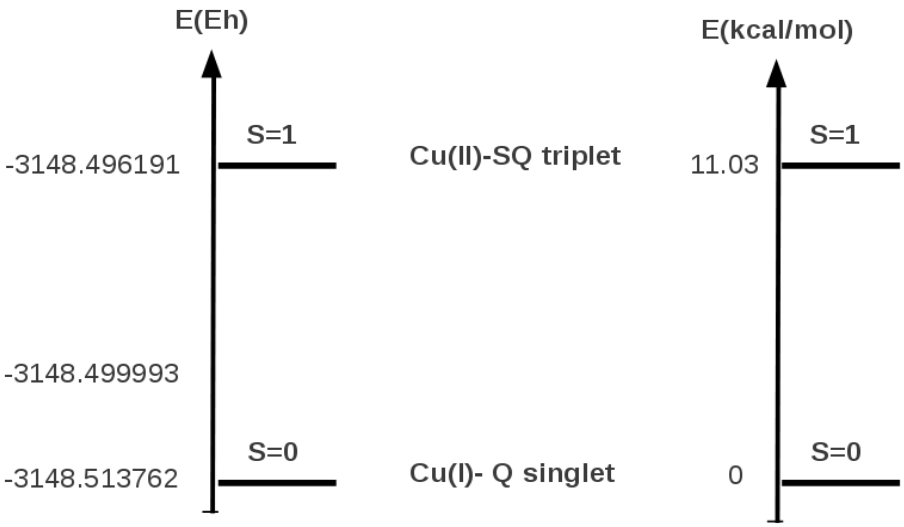

Figure S17. Energetic analysis of the DFT calculations for **2**.

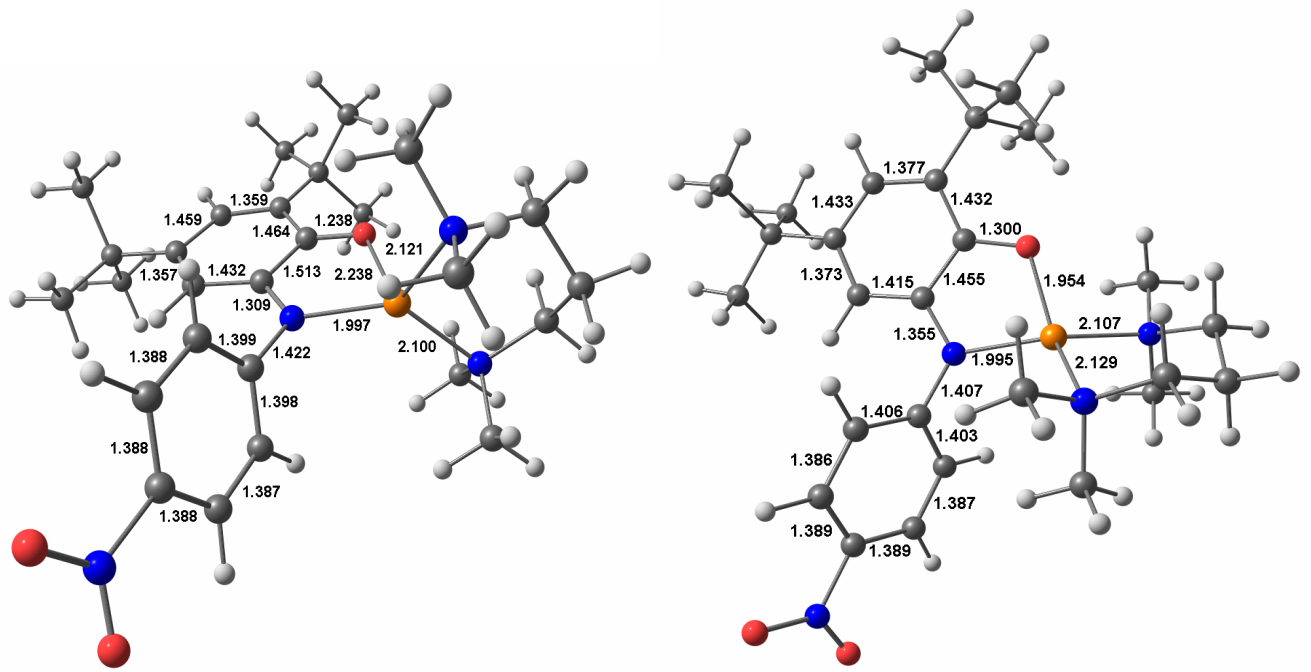

Figure S18. Optimized structures of singlet cation **2** (left) and triplet cation **2** (right) together with interatomic distances.

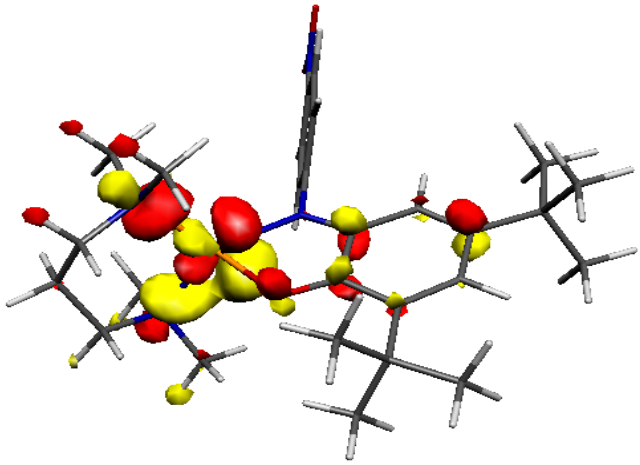

Figure S19. HOMO of singlet cation **2**.

Table S5. Calculated electronic transtisions of singlet cation **2**.

Transition	λ^{calc} (nm)	f^{calc}	Assignment	λ^{expt} (nm)	ε (M^{-1} cm^{-1})
1	720	0.112	MLCT	713	7500
2	613	0.129	MLCT	556	2800
3	351	0.082	LLCT	328	8100

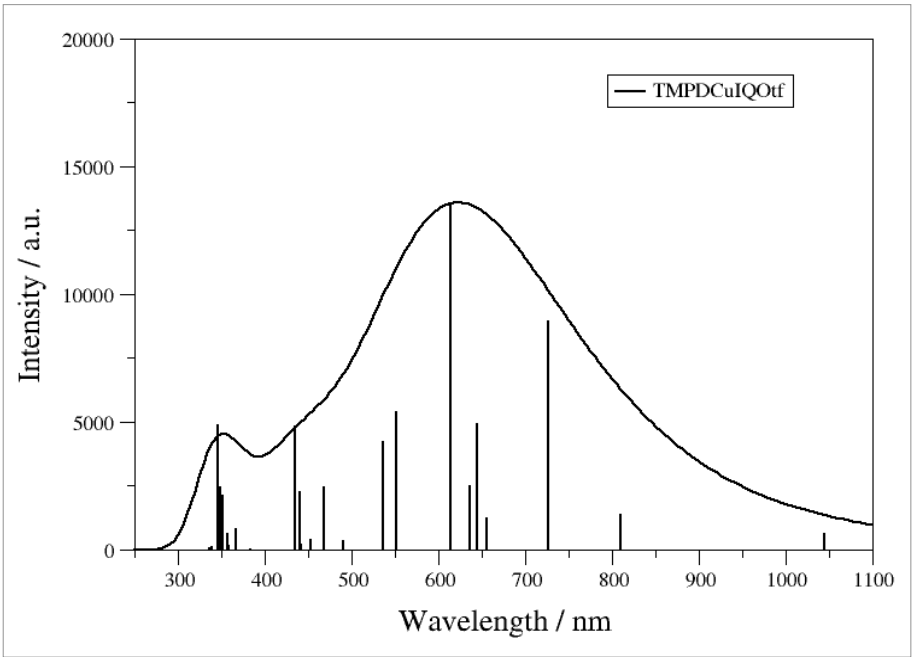

Figure S20. Theoretical fit of the UV-vis spectrum of singlet cation **2**.

Transition 1

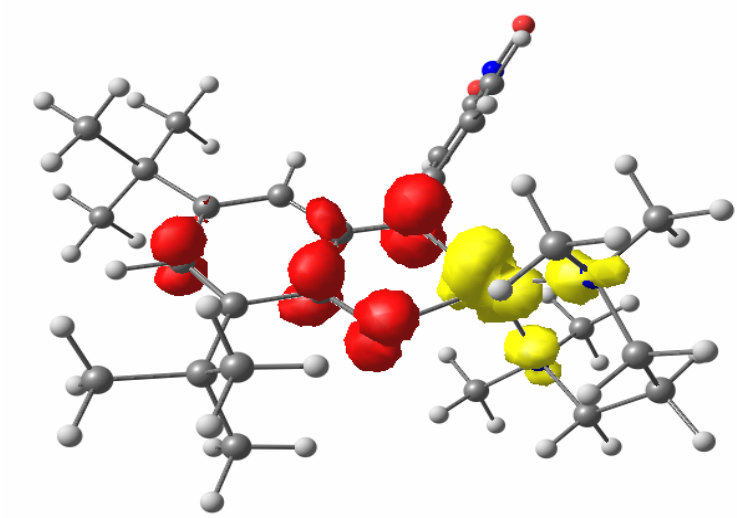

Transition 2

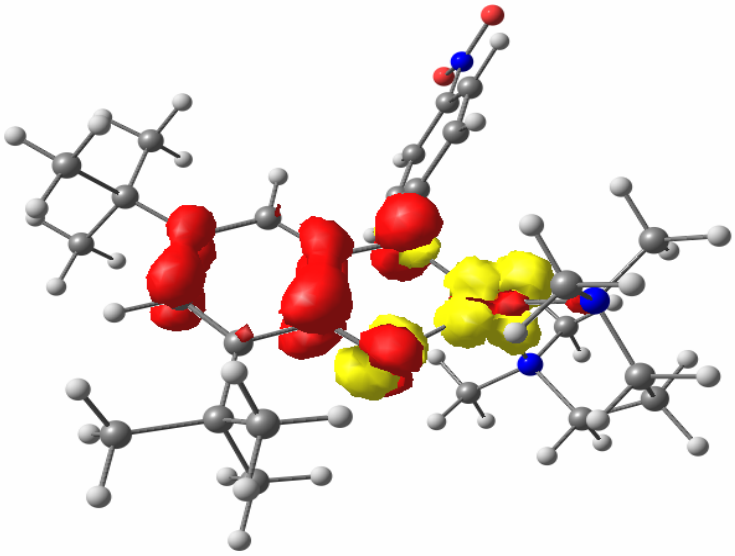

Transition 3

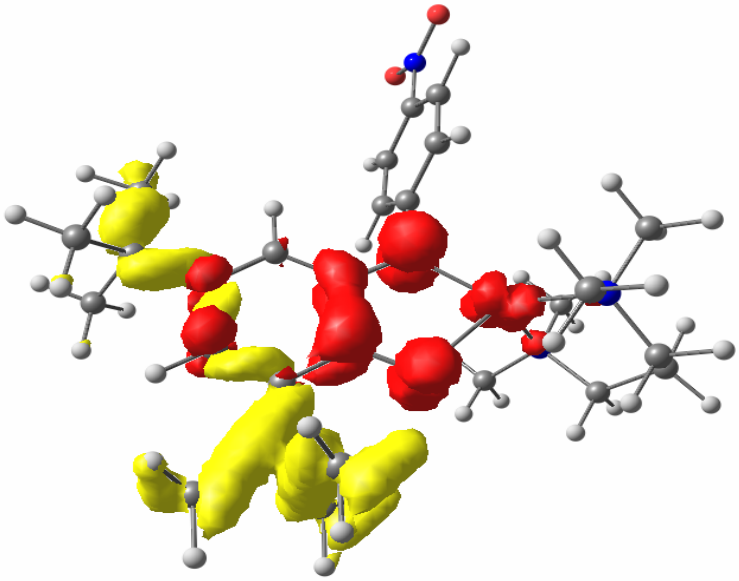

Figure S21. Difference electron densities sketch of transitions 1-3 for singlet cation **2** (yellow = negative, red = positive).

References

[1] G. J. Kubas, *Inorg. Synth.* **1990**, *28*, 68-70.
[2] I. Halasz, I. Biljan, P. Novak, E. Meštrović, J. Plavec, G. Mali, V. Smrečki, H. Vančik, *J. Mol. Struct.* **2009**, *918*, 19-25.
[3] J. Rosevear, J. Wilshire, *Aust. J. Chem.* **1985**, *38*, 723-733.
[4] Neese, F. Wiley; *Interdiscip. Rev. Comput. Mol. Sci.* **2012**, *2*, 73.
[5] Perdew, *J. P. Phys. Rev. B*; **1986**, *33*, 8822.
[6] Perdew, *J. P. Phys. Rev. B*; **1986**, *34*, 7406.
[7] Becke, A. D. *Phys. Rev. A*; **1988**, *38*, 3098.
[8] Schäfer, A.; Huber, C.; Ahlrichs, R.; *J. Chem. Phys.* **1994**, *100*, 5829.
[9] Neese, F. J.; *Comput. Chem.* **2003**, *24*, 1740.
[10] Weigend, F.; *Phys. Chem. Chem. Phys.* **2006**, *8*, 1057.
[11] Klamt, A.; Schürmann, G. *J.*; *Chem. Soc., Perkin Trans. 2*, **1993**, 799.
[12] Becke, A. D.; *J. Chem. Phys.* **1993**, *98*, 1372.
[13] Lee, C. T.; Yang, W. T.; Parr, R. G.; *Phys. Rev. B,* **1988**, *37*, 785.
[14] L. Noodleman; *J. Chem. Phys.*; **1981,** *74*, 5737.
[15] L. Noodleman, D. A. Case; *Adv. Inorg. Chem.* **1992,** *38*, 423.
[16] L. Noodleman, E. R. Davidson; *Chem. Phys.* **1986,** *109*, 131.
[17] T. Soda, Y. Kitagawa, T. Onishi, Y. Takano, Y. Shigeta, H. Nagao, Y. Yoshika, K. Yamaguchi; *Chem. Phys. Lett.* **2000**, 223.
[18] K. Yamaguchi, Y. Takahara, T. Fueno, In *Applied Quantum Chemistry*, *V*, V. H. Smith, Ed. Reidel: Dordrecht, **1986**.
[19] W. Heisenberg; *Z. Physik* **1926,** *38*, 411.
[20] W. Heisenberg; *Z. Physik* **1928,** *49*, 619.
[21] P. A. M. Dirac; *Proc. Roy. Soc.* **1929,** *A123*, 714.
[22] J. H. Van Vleck; *The Theory of Electronic and Magnetic Susceptibilities*. Oxford University: London **1932**.
[23] Casida, M. E., In *Recent Advances in Density Functional Methods*, Chong, D.P. Ed. World Scientific: Singapore, **1995**.
[24] Stratmann, R. E.; Scuseria, G. E.; Frisch, M. J.; *J. Chem. Phys.* **1998,** *109*, 8218-8224.
[25] Bauernschmitt, R.; Ahlrichs, R.; *Chem. Phys. Lett.* **1996**, 454-464.
[26] Hirata, S.; Head-Gordon, M.; *Chem. Phys. Lett.* **1999,** *314*, 291-299.
[27] Hirata, S.; Head-Gordon, M.; *Chem. Phys. Lett.* **1999,** *302*, 375-382.
[28] Neese, F.; *J. Chem. Phys*. **2001**, *115*, 11080.
[29] chemcraft http://chemcraftprog.com.